Chinese Physics Letters **40**, 014201 (2023)

Flat Top Optical Frequency Combs Based on a Single-Core Quantum Cascade Laser at Wavelength of ∼8.7 μm

Yu Ma(马钰)[1,2], Wei-Jiang Li(李伟江)[1,2], Yun-Fei Xu(许云飞)[1,2], Jun-Qi Liu(刘俊岐)[1,2*], Ning Zhuo(卓宁)[1,2*], Ke Yang(杨科)[1,2], Jin-Chuan Zhang(张锦川)[1,2], Shen-Qiang Zhai(翟慎强)[1,2], Shu-Man Liu(刘舒曼)[1,2], Li-Jun Wang(王利军)[1,2], and Feng-Qi Liu(刘峰奇)[1,2]

[1]*Key Laboratory of Semiconductor Materials Science, and Beijing Key Laboratory of Low Dimensional Semiconductor Materials and Devices, Institute of Semiconductors, Chinese Academy of Sciences, Beijing 100083, China*
[2]*Center of Materials Science and Optoelectronics Engineering, University of Chinese Academy of Sciences, Beijing 100049, China*

(Received 12 October 2022; accepted manuscript online 23 November 2022)

We present optical frequency combs with a spectral emission of 48 cm^{-1} and an output power of 420 mW based on a single-core quantum cascade laser at $\lambda \sim 8.7$ μm. A flat top spectrum sustains up to 130 comb modes delivering ∼3.2 mW of optical power per mode, making it a valuable tool for dual comb spectroscopy. The homogeneous gain medium, relying on a slightly diagonal bound-to-continuum structure, promises to provide a broad and stable gain for comb operating. Remarkably, the dispersion of this device is measured within 300 fs^2/mm to ensure stable comb operation over 90% of the total current range. The comb is observed with a narrow beatnote linewidth around 2 kHz and has weak dependence on the applied current for stable comb operation.

DOI: 10.1088/0256-307X/40/1/014201

Optical frequency combs (OFCs) are promising light sources for many revolutionary applications due to their high stability and low phase noise.[1,2] Recently, novel methods based on optical frequency combs[3–5] have opened new possibilities in the fields of trace gas-sensing, remote-sensing and laser spectroscopy. Especially in the mid-infrared (MIR) and terahertz (THz) regions, due to the fact that the fundamental roto-vibrational bands of a variety of molecules lie with absorption strength higher than those in the visible or near-infrared, intense development of OFCs is mainly driven by their applications in high-resolution spectroscopy. The recently developed quantum cascade laser (QCL) frequency combs[6–8] are especially attractive, which can adjust emitting wavelength by changing the thickness and components of the materials and cover from MIR to THz spectrum range (3–300 μm). Due to the inherently high optical nonlinearity of the quantum engineered gain medium, the comb formation takes place directly in the QCL active region,[1,9,10] which offer the possibility of completely integrated chip-based sources and have advantages for mass production using standard semiconductor technologies.[11] Shortly after their demonstrations, dual-comb spectroscopy based on QCL OFCs is proven to be the potentially promising applications in high spectral resolution and fast scanning.[12–14]

In order to promote the dual comb spectroscopy, key characteristics of QCL combs,[15] such as stable comb operating, flat and broad spectral range, wide current dynamic range, high power-per-mode, still need to be improved. Recent experiments showed that dispersion in QCLs can be compensated for by canceling the positive cavity dispersion for stable comb operating by depositing Gires–Tournois mirror[16,17] on the back-facet of devices. However, due to the multi-layer dielectrics required, Gires–Tournois mirror technique is difficult for long wavelength. Heterogeneous multistacked active regions[18,19] are ideal for broadening the laser spectra, which requires judicial designs to match the threshold currents between the different active region modules. In such a way, stacking dissimilar active regions can achieve a relatively flat gain top, within which the intrinsic dispersion is small enough to form comb operation. To date, other approaches, such as multi-section waveguides[20] or coupled waveguides,[21] have been proved to be the effective ways for stable comb operating with wide spectral coverage. On the whole, the improvements of key characteristics for QCL combs, of course, rely on the feasibility of such technologies, which at present are not comprehensive but an active area of development.

Therefore, in this Letter we propose a slightly diagonal bound-to-continuum (BTC) single-core structure to get flat and stable QCL OFCs at $\lambda \sim 8.7$ μm, assisting frequency comb operation over 90% of the total current range. The QCL combs span a spectral emission about 48 cm^{-1} with the output power as high as 420 mW. A flat spectrum ensures up to 130 comb modes delivering ∼3.2 mW of optical power per mode. In addition, the device is observed with a narrow intermode beatnote linewidth around 2 kHz and has weak dependence on the applied current for stable comb operation. Using Fourier transform spectroscopy,

*Corresponding authors. Email: jqliu@semi.ac.cn; zhuoning@semi.ac.cn
© 2023 Chinese Physical Society and IOP Publishing Ltd

the group velocity dispersion (GVD) of this device below threshold proves to be within 300 fs^2/mm. Depending on four-wave mixing (FWM) as a phase-locking mechanism, broadband QCLs with low enough values of GVD can accomplish stable OFC operating.

The material structure of our comb was grown with the molecular beam epitaxial method on an n-InP (Si, $1 \times 10^{17}\,cm^{-3}$) substrate. The layer sequence of one active region stage starting from the injection barrier in nm is **4.1**/1.4/**1**/5.2/**1.1**/5.2/**1**/4.8/**1.7**/3.7/**2.3**/3/**1.9**/2.8/**2**/2.7/**2.1**/2.5/**2.6**/2.6/**3.3**/2.4, where the $In_{0.523}Al_{0.477}As$ barriers are in bold font and the $In_{0.532}Ga_{0.468}As$ wells are in normal font. The underlined layers are doped to $n = 2.5 \times 10^{17}\,cm^{-3}$. The QCL structure is based on a slightly diagonal BTC design with four coupled wells as shown in Fig. 1(a). At the design bias of 45 kV/cm, electrons are injected into the upper level 4 from the injector level g' by resonant tunneling. The thickness of the injected barrier is appropriately chosen, which obtains a high coupling strength ($\hbar\Omega \approx 4.8$ meV) between the upper lasing level 4 and the ground injector level g' to achieve a moderate current density dynamic range and high output power. Benefiting from BTC design, the lasers are generated through a modified diagonal transition from the bound level 4 to the miniband. As the transition energies have slightly different values, this design will naturally broaden the lasing bandwidth. Simultaneously, the moderately enhanced main transition of 4–3 in BTC diagonal transitions guarantees a broad and flat gain spectrum, sustaining laser operation in an important number of longitudinal modes. Moreover, the slightly diagonal scheme features high laser transition matrix elements with strong coupling between the lower lasing levels and injector levels ($Z_{43} = 2.63$ nm, $Z_{42} = 0.53$ nm, $Z_{41} = 0.23$ nm), resulting in large nonlinear susceptibilities. In this case, the calculated upper laser lifetime for this design is $\sim$1.08 ps. In theory, FWM combined with the short gain recovery time prompts QCL to operate in the self-frequency-modulated regime characterized by stable coherent combs in the frequency domain.[1] This design for the relatively thick period length and the slightly diagonal nature of the laser transition also guarantees small changes of the emission with increasing voltage due to the weakened linear Stark shift effect. The model predicts accurately the field dependence of these peaks, as shown in Fig. 1(b). These peaks, correlated at low fields (37–41 kV/cm), smoothed at higher bias (41–47 kV/cm). It can be found that under the high bias part, the gain range shift from the bound state 4 to the lower state 3 is very small, which is conducive to achieve a stable gain. The optimized band structure guarantees a broad and stable gain spectrum after loss clamped, to reduce or compensate the dispersion for comb operation. On the other hand, this structure takes the advantage of the four-coupled-well design for high device performance. Because of ensuring a resonant tunneling injection by achieving a large penetration of the upper state into the injection barrier, it helps to bring high population inversion and to achieve high power.

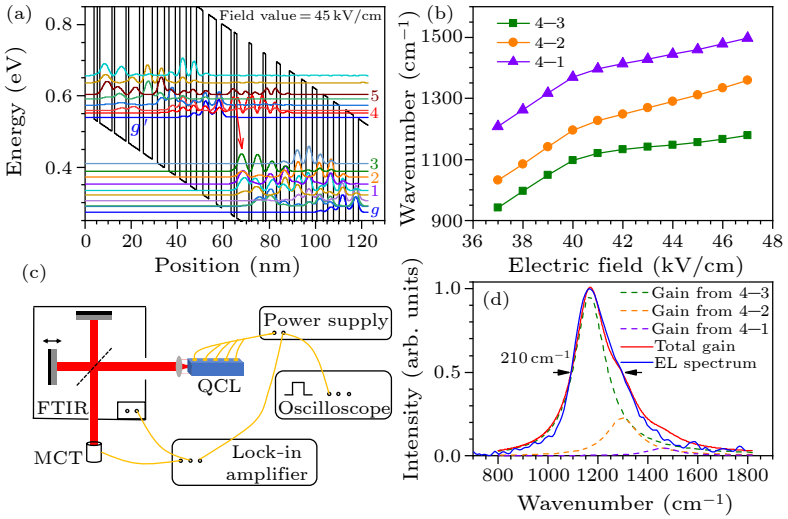

Fig. 1. (a) Conduction band diagram and energy level profile of a $\lambda \sim 8.7$ µm QCL structure at an electric field of 45 kV/cm. (b) The field dependence of gain peaks from the bound level 4 to the miniband (levels 3, 2 and 1). (c) Setup used to acquire the EL spectrum generated by the QCL comb biased below threshold. (d) Measured and calculated gain. Solid blue line: the EL spectrum. Solid red line: total gain. Dashed lines: the gain from the bound level 4 to the miniband (levels 3, 2 and 1) are shown in green, yellow and purple, respectively.

The overall material structure from the InP substrate (Si, $1 \times 10^{17}\,cm^{-3}$) consists of 2 µm (Si, $4 \times 10^{16}\,cm^{-3}$) and 3 µm (Si, $2 \times 10^{16}\,cm^{-3}$) InP buffer layers, a 40-period active region (Si, $\sim 2.5 \times 10^{17}\,cm^{-3}$) sandwiched between two 200 nm InGaAs (Si, $6 \times 10^{16}\,cm^{-3}$) confinement layers, a 3.2 µm InP cladding layer (Si, $2 \times 10^{16}\,cm^{-3}$) and 0.6 µm highly doped InP cap layer (Si, $5 \times 10^{18}\,cm^{-3}$). The device was processed to a buried heterostructure QCL. A 12-µm-wide ridge was etched by wet-etching technique and a lateral InP:Fe insulating layer was grown by metalorganic

chemical vapor deposition. Finally, laser bars for length of 4 mm were then indium soldered on a copper plate with wire bonded by epilayer-down mounting.

In order to reflect the information of the internal energy level of the laser, we measured electroluminescence (EL) spectra of this device using a Fourier transform infrared (FTIR) spectrometer with 2 cm^{-1} resolution in step-scan mode with a cryogenically cooled mercury cadmium telluride (MCT) detector and a lock-in signal recovery scheme [see Fig. 1(c)]. The resulting spectra of a 12-μm-wide and 4-mm-long sample at room temperature under the injection current of 0.45 A. The linewidth of the spectra taken with pulsed injection currents of 5 μs width at a repetition rate of 20 kHz is observed to be very wide value of 210 cm^{-1} [see Fig. 1(d)]. As it can be seen, for this electric field, the spontaneous emission mainly shows three relevant gain peaks. The first one, placed at 143.5 meV, can be attributed to the lasing transition 4–3 while the other two, respectively, at 162.6 meV and 181.1 meV, are relative to the transition from the bound state 4 to the two lower states 2 and 1. The data between 800 and 1600 cm^{-1} could be well fitted by a sum of three Gaussians from the bound level 4 to the levels (3,2,1), respectively, in good agreement with the computed transition energies. We believe that the asymmetry of the gain comes from the contributions of the bound state and other lower states, due to the fact that the oscillator strength spreads over several lower states. The nonlinearity allowing FWM originates from the resonant optical transitions in the BTC design and asymmetry of the gain.[1,12,22] Longitudinal modes from the resonant cavity are locked by FWM to establish a fixed phase relation among them and ensure a coherent OFCs operation.

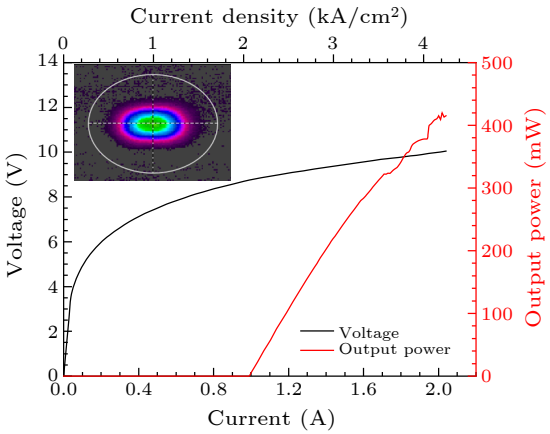

Fig. 2. The P–I–V characteristics of the 12-μm-wide and 4-mm-long device at 300 K in the CW mode. Inset: the beam profile of the QCL measured at 300 K under a current of 1.6 A with a duty cycle of 2% (10 kHz, 2 μs).

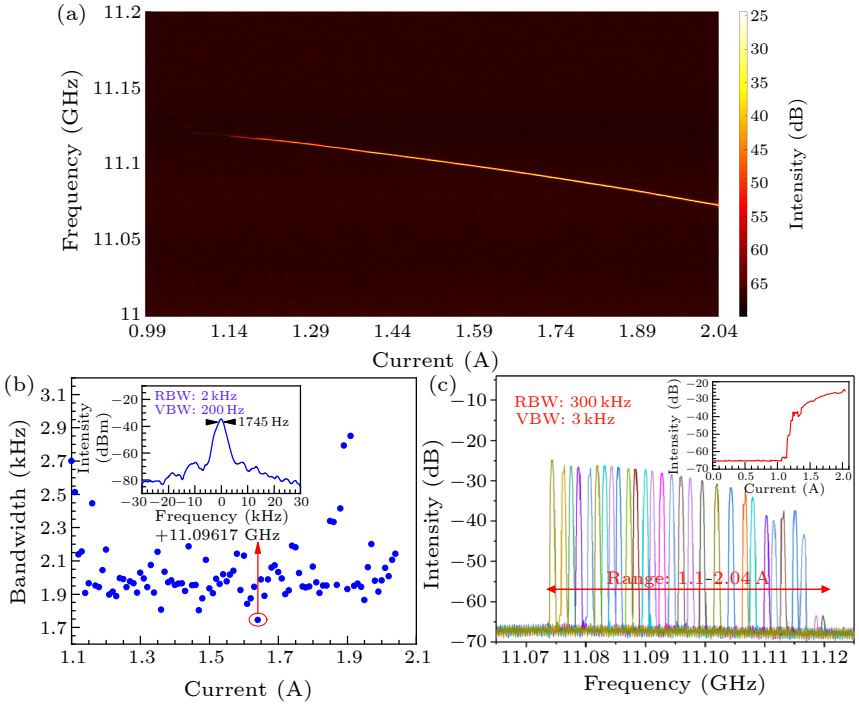

Fig. 3. (a) Free running beatnote mapping as a function of drive current measured at 300 K in CW mode. The resolution bandwidth is set as 300 kHz and the resolution bandwidth is 3 kHz. (b) Intermode beatnote linewidth measured at 300 K as a function of the driving current. Inset: the narrowest beatnote linewidth at 1.65 A. (c) Beatnote spectra (1.1–2.04 A) at 300 K. Inset: signal-to-noise ratio of the intermode beatnote as a function of the driving current.

To ensure the smooth operating at the constant temperature, the device coated with silicone grease at the bottom is installed on the water-cooling platform with thermoelectric cooler for temperature control. The thermistor is closely connected to them for real-time temperature adjustment. Figure 2 shows the power–current–

voltage (P–I–V) characteristic, measured with driving the QCL in continuous-wave (CW) mode by a power supply (THORLABS ITC4005QCL) and the pyroelectric power meter (Molectron, EPM1000). At 300 K, the CW threshold current is 1 A, the maximum current is 2.04 A, and the maximum peak optical power is 420 mW. For the 12-μm-wide and 4-mm-long device, the CW threshold current density is 2.08 kA·cm^{-2} and the maximum current density is 4.25 kA·cm^{-2}, so the operational dynamic range is 2.04. The beam profile of the laser with lens (Lightpath,390037IR1) collimation at a current of 1.6 A with a duty cycle of 2% is shown in the illustration of Fig. 2. The profile is taken with a pyroelectric camera placed 60 cm away from the laser. The beam consists of a pure zero order mode TM_{00}.

In order to explore the comb operation, an intermode beatnote is detected to characterize the coherence properties at 300 K by an RF spectral analyzer (MXA Signal Analyzer N9020 A). Figure 3(a) plots the beatnote spectra at different currents. The spectra were acquired using a spectrum analyzer with resolution bandwidth (RBW) of 300 kHz and video bandwidth (VBW) of 3 kHz. A single beatnote signal appears at 1.1 A and persists continuously until 2.04 A, over 90% of entire laser emitting range from the threshold to the roll-over currents, which is much wider than the previous demonstrations.[20,21] The intermode beatnote frequency tuned smoothly with current at a rate of −47.9 kHz/mA, from 11.12 GHz to 11.075 GHz at the comb range (1.1–2.04 A), which has weak dependence on the applied current. As the current increased, so did the beatnote signal. The highest signal noise ratio (SNR) was 41 dB in Fig. 3(c) with no significant side peaks, indicating a low-noise operation of the comb. The narrowest beatnote linewidth at 1.65 A was 1745 Hz in Fig. 3(b). Beatnote linewidths are in the range of 1.7–2.9 kHz, and most of the values are stable at about 2 kHz, with a relatively narrow linewidth. Remarkably, the comb does not show any multi-beatnote regime.

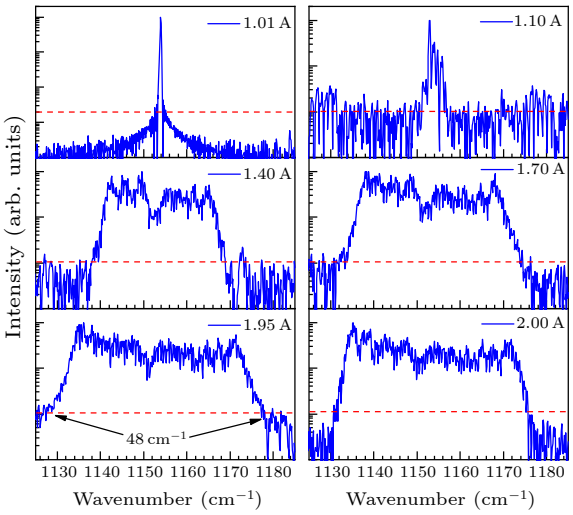

Fig. 4. The lasing spectra of the 4-mm-long device at 300 K at various injection currents.

Lasing spectra of the devices in CW operation were acquired by Fourier transform infrared spectra (FTIR) with a spectral resolution of 0.125 cm^{-1} at different currents at 300 K. As shown in Fig. 4, the device is initially emitting on a single frequency mode (∼1154 cm^{-1}) at the threshold and then turned to multimode at 1.1 A with a series of equidistant optical modes spaced by the cavity round-trip frequency. The widest spectral coverage reached 48 cm^{-1} at 1.95 A. A flat bandwidth with a power of 420 mW is achieved, corresponding to 130 optical active laser modes. Under this condition, the average optical power per optical mode is ∼3.2 mW. As predicted from our design results, the slightly diagonal BTC design with four coupled wells could significantly broaden the gain linewidth and improve the device performance. It is observed that at a certain pumping current above lasing threshold, QCLs operate in CW mode and develop a mode proliferation mainly due to the spatial-hole-burning (SHB) effect which is inspired when the intensity of the field in the cavity is high. Remarkably, the spectrum extends equably on both sides of the gain peak as the injection current increases. The appearance of a single beat signal indicates that the active region with low Stark effect forms a flat top optical comb under a large current dynamic range. This flat top optical comb regime is characterized by a broadband optical spectrum (48 cm^{-1}) and a narrow (∼2 kHz) frequency beatnote linewidth in the RF spectrum at the cavity round-trip frequency. In other words, the phase relationships between the longitudinal modes in this flat and broad spectrum are stable. Hence, on the one hand the broad gain and SHB in QCL support multimode operation, on the other hand, short gain recovery time leads to a self-frequency modulated operation by FWM.

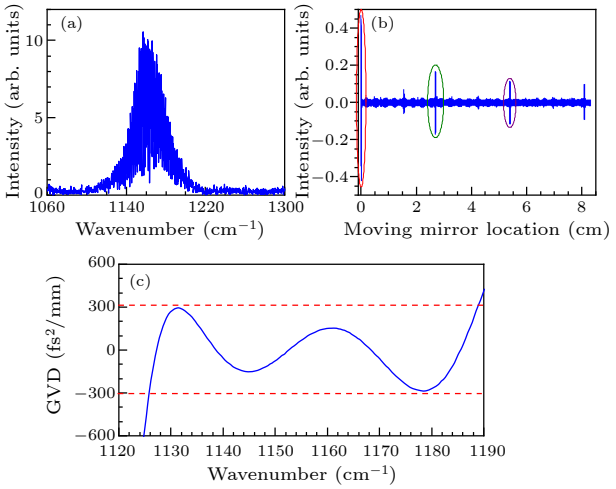

Fig. 5. (a) Subthreshold spontaneous emission spectrum. (b) Corresponding interferogram of the 4-mm-long device measured at a resolution of 0.125 cm^{-1} at 300 K. (c) The calculated GVD.

Group velocity dispersion (GVD) plays an important role in the degradation of QCL combs. In free-running QCLs, due to their broadband nature and ultrafast carrier dynamics, there will be a strong competition between FWM and GVD for comb operation. To get a deeper insight on the device with the current range of more than

90% for comb operating, the method of calculating the dispersion curves by subthreshold spontaneous emission spectrum[23] in Fig. 5(a) is performed in the FTIR employing MCT as a detector. For acquiring a good SNR, the device is matched with lens collimation and temperature controlling. The lights emitting directly from the cavity and traveling one more roundtrip inside the resonator, corresponding to 0^{th} order satellite peak (red circle) and 1^{st} order satellite peak (green circle) in the electroluminescence interferograms, are obtained to analyze the dispersion information in Fig. 5(b). For the device with a 4-mm-long cavity, the dispersion information can be expressed as

$$\text{GVD} = \frac{1}{L}\frac{\partial^2(\varphi_{0\text{th}} - \varphi_{1\text{st}})}{\partial\omega^2}, \tag{1}$$

where φ is the phase defined as $\varphi = k(\omega)z$ with the wave number $k(\omega)$. Figure 5(c) shows the calculated GVD. In the vicinity of the central wavelength, GVD is maintained nearly within $300\,\text{fs}^2/\text{mm}$. Around $1130\,\text{cm}^{-1}$ and $1180\,\text{cm}^{-1}$, GVD is slightly higher, whereas it has less influence on comb operating due to far away from the central wavelength. In general, the calculated GVD values are smaller than the previous demonstrations ($\sim 500\,\text{fs}^2/\text{mm}$). Depending on FWM as a phase-locking mechanism, broadband QCLs with low enough values of GVD can accomplish stable comb operating under a large current range ($> 90\%$).

In summary, we have demonstrated flat top optical frequency combs over a nearly full current range based on a single-core quantum cascade laser at $\lambda \sim 8.7\,\mu\text{m}$. The active region is based on a slightly diagonal BTC structure with four wells coupled to get broad and stable gain. We performed the GVD measurements by means of Fourier transform spectroscopy and demonstrated that it is maintained nearly within $300\,\text{fs}^2/\text{mm}$. Depending on FWM as a phase-locking mechanism, broadband QCLs with low GVD prompts stable comb operation. Remarkably, the frequency comb dynamic current range over the entire laser emitting range is estimated to be 90%. The output power of the comb is as high as 420 mW with optical spectra up to $48\,\text{cm}^{-1}$. A flat spectrum ensures up to 130 comb modes delivering $\sim 3.2\,\text{mW}$ of optical power per mode. The comb provides useful insight on dual comb technology for high resolution spectroscopy at MIR region.

Acknowledgments. The authors would like to thank P. Liang and Y. Hu for their help in device fabrication processing. This work was supported by the National Natural Science Foundation of China (Grant Nos. 61734006, 61835011, 61991430, and 62174158), the Youth Innovation Promotion Association of the Chinese Academy of Sciences (Grant No. 2021107), and the Key Program of the Chinese Academy of Sciences (Grant Nos. XDB43000000, YJKYYQ20190002, and QYZDJ-SSW-JSC027).

References

[1] Hugi A, Villares G, Blaser S, Liu H C, and Faist J 2012 *Nature* **492** 229
[2] Soibel A, Capasso F, Gmachl C, Peabody M L, Sergent A M, Paiella R, Hwang H Y, Sivco D L, Cho A Y, Liu H C, Jirauschek C, and Kartner F X 2004 *IEEE J. Quantum Electron.* **40** 844
[3] Faist J, Villares G, Scalari G, Rösch M, Bonzon C, Hugi A, and Beck M 2016 *Nanophotonics* **5** 272
[4] Villares G, Hugi A, Blaser S, and Faist J 2014 *Nat. Commun.* **5** 5192
[5] Hillbrand J, Andrews A M, Detz H, Strasser G, and Schwarz B 2019 *Nat. Photon.* **13** 101
[6] Liu J Q, Chen J Y, Liu F Q, Li L, Wang L J, and Wang Z G 2010 *Chin. Phys. Lett.* **27** 104205
[7] Wang T, Liu J Q, Chen J Y, Liu Y H, Liu F Q, Wang L J, and Wang Z G 2013 *Chin. Phys. Lett.* **30** 064201
[8] Fei T, Zhai S, Zhang J, Zhuo N, Liu J, Wang L, Liu S, Jia Z, Li K, Sun Y, Guo K, Liu F, and Wang Z 2021 *J. Semicond.* **42** 112301
[9] Beiser M, Opačak N, Hillbrand J, Strasser G, and Schwarz B 2021 *Opt. Lett.* **46** 3416
[10] Lu Q Y, Razeghi M, Slivken S, Bandyopadhyay N, Bai Y, Zhou W J, Chen M, Heydari D, Haddadi A, McClintock R, Amanti M, and Sirtori C 2015 *Appl. Phys. Lett.* **106** 051105
[11] Chang L, Liu S, and Bowers J E 2022 *Nat. Photon.* **16** 95
[12] Consolino L, Nafa M, De Regis M, Cappelli F, Garrasi K, Mezzapesa F P, Li L, Davies A G, Linfield E H, Vitiello M S, Bartalini S, and De Natale P 2020 *Commun. Phys.* **3** 69
[13] Li H, Li Z, Wan W, Zhou K, Liao X, Yang S, Wang C, Cao J C, and Zeng H 2020 *ACS Photon.* **7** 49
[14] Jerez B, Martín-Mateos P, Prior E, de Dios C, and Acedo P 2016 *Opt. Express* **24** 14986
[15] Garrasi K, Mezzapesa F P, Salemi L, Li L, Consolino L, Bartalini S, De Natale P, Davies A G, Linfield E H, and Vitiello M S 2019 *ACS Photon.* **6** 73
[16] Razeghi M, Lu Q, Wu D, and Slivken S 2018 *Proc. SPIE* **10756** 107560I
[17] Villares G, Riedi S, Wolf J, Kazakov D, Süess M J, Jouy P, Beck M, and Faist J 2016 *Optica* **3** 252
[18] Li L H, Garrasi K, Kundu I, Han Y J, Salih M, Vitiello M S, Davies A G, and Linfield E H 2018 *Electron. Lett.* **54** 1229
[19] Jouy P, Wolf J M, Bidaux Y, Allmendinger P, Mangold M, Beck M, and Faist J 2017 *Appl. Phys. Lett.* **111** 141102
[20] Wang R J, Täschler P, Kapsalidis F, Shahmohammadi M, Beck M, and Faist J 2020 *Opt. Lett.* **45** 6462
[21] Bidaux Y, Kapsalidis F, Jouy P, Beck M, and Faist J 2018 *Laser Photon. Rev.* **12** 1700323
[22] Corrias N, Gabbrielli T, De Natale P, Consolino L, and Cappelli F 2022 *Opt. Express* **30** 10217
[23] Hofstetter D and Faist J 1999 *IEEE Photon. Technol. Lett.* **11** 1372